Symmetrical and Unsymmetrical Dicopper Complexes Based on Bis-Oxazoline Units: Synthesis, Spectroscopic Properties and Reactivity

James A Isaac, Gisèle Gellon, Florian Molton, Christian Philouze, Nicolas Le Poul, Catherine Belle, Aurore Thibon-Pourret

inorganics

MDPI

Article

Symmetrical and Unsymmetrical Dicopper Complexes Based on Bis-Oxazoline Units: Synthesis, Spectroscopic Properties and Reactivity

James A. Isaac [1], Gisèle Gellon [1], Florian Molton [1], Christian Philouze [1], Nicolas Le Poul [2], Catherine Belle [1,*] and Aurore Thibon-Pourret [1,*]

[1] Université Grenoble-Alpes, CNRS, Department of Molecular Chemistry (DCM, UMR 5250), 38058 Grenoble, CEDEX 9, France; james.alfisaac@gmail.com (J.A.I.); florian.molton@univ-grenoble-alpes.fr (F.M.); christian.philouze@univ-grenoble-alpes.fr (C.P.)
[2] Université de Bretagne Occidentale, CNRS, Laboratoire de Chimie, Electrochimie Moléculaires et Chimie Analytique (CEMCA, UMR 6521), 29238 Brest, CEDEX 3, France; lepoul@univ-brest.fr
* Correspondence: catherine.belle@univ-grenoble-alpes.fr (C.B.); aurore.thibon@univ-grenoble-alpes.fr (A.T.-P.)

Abstract: Copper–oxygen adducts are known for being key active species for the oxidation of C–H bonds in copper enzymes and their synthetic models. In this work, the synthesis and spectroscopic characterizations of such intermediates using dinucleating ligands based on a 1,8 naphthyridine spacer with oxazolines or mixed pyridine-oxazoline coordination moieties as binding pockets for copper ions have been explored. On the one hand, the reaction of dicopper(I) complexes with O_2 at low temperature led to the formation of a μ-η^2:η^2 Cu_2:O_2 peroxido species according to UV-Vis spectroscopy monitoring. The reaction of these species with 2,4-di-tert-butyl-phenolate resulted in the formation of the C–C coupling product, but no insertion of oxygen occurred. On the other hand, the synthesis of dinuclear Cu(II) bis-μ-hydroxido complexes based on pyridine–oxazoline and oxazoline ligands were carried out to further generate $Cu^{II}Cu^{III}$ oxygen species. For both complexes, a reversible monoelectronic oxidation was detected via cyclic voltammetry at $E_{1/2}$ = 1.27 and 1.09 V vs. Fc^+/Fc, respectively. Electron paramagnetic resonance spectroscopy (EPR) and UV-Vis spectroelectrochemical methods indicated the formation of a mixed-valent $Cu^{II}Cu^{III}$ species. Although no reactivity towards exogeneous substrates (toluene) could be observed, the $Cu^{II}Cu^{III}$ complexes were shown to be able to perform hydroxylation on the methyl group of the oxazoline moieties. The present study therefore indicates that the electrochemically generated $Cu^{II}Cu^{III}$ species described herein are capable of intramolecular aliphatic oxidation of C–H bonds.

Keywords: copper-bioinspired chemistry; mixed-valent $Cu^{II}Cu^{III}$ species; dioxygen activation

Citation: Isaac, J.A.; Gellon, G.; Molton, F.; Philouze, C.; Le Poul, N.; Belle, C.; Thibon-Pourret, A. Symmetrical and Unsymmetrical Dicopper Complexes Based on Bis-Oxazoline Units: Synthesis, Spectroscopic Properties and Reactivity. *Inorganics* **2023**, *11*, 332. https://doi.org/10.3390/inorganics11080332

Academic Editor: Gianella Facchin

Received: 6 July 2023
Revised: 28 July 2023
Accepted: 8 August 2023
Published: 11 August 2023

1. Introduction

An important part of the research in bio-inorganic chemistry is currently focused on the development of model complexes that mimic the catalytic center of enzymes. In the field of copper-metalloenzymes, low-temperature oxygenation of synthetic Cu^I or Cu^I_2 compounds has provided a variety of structurally and spectroscopically characterized Cu_2O_2 species including high valent species [1] (Scheme 1). The combination with their respective reactivity profiles has provided useful information on dicopper-metalloenzyme structure and function [2,3]. In particular, Cu_2-containing enzymes activate O_2 to generate Cu_2O_2 species capable of oxidizing various substrates varying from catechol to methane [4]. To prepare model complexes, the nature of the supporting ligands employed, the presence of substituents to control the bulkiness and the electronic properties (donor/acceptor groups) and flexibility of the ligand control the final structure of the Cu_2O_2 species. The majority of dinucleating ligands with tridentate arms described in the literature have been used to generate bis-μ-oxido dicopper(III) complex or equilibrium mixtures of (μ-η^2:η^2)

peroxido dicopper(II) and bis-μ-oxido species [5–10] (Scheme 1). By contrast, dinucleating ligands with tetradentate arms have predominantly led to cis-μ-1,2-peroxido dicopper(II) complexes [11] or trans-μ-1,2-peroxido-dicopper(II) complexes [12–16].

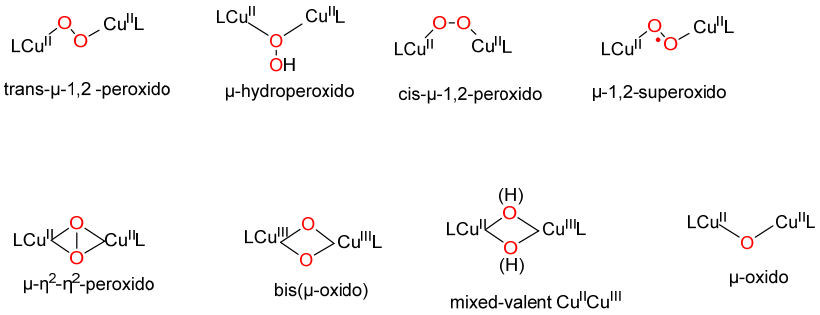

Scheme 1. Representative Cu_2/O_2 adducts characterized from model complexes.

In this context, we reported the synthesis of the symmetrical **Cu_2Py_4** complex (**Py_4** ligand is presented on Scheme 2) containing a naphthyridine spacer (known to be redox-inert, and to promote two well-defined coordination sites with a short metal-metal distance) associated with bis-pyridyl arms [17]. With the **Cu_2Py_4** bis(μ-hydroxido) complex, we showed that a mixed valent $Cu^{II}Cu^{III}$ intermediate could be generated and activate strong sp^3 C–H bonds [18]. In addition, from the corresponding dinuclear **$Cu^{I}{}_2Py_4$** species, no O_2 adduct was detected [19].

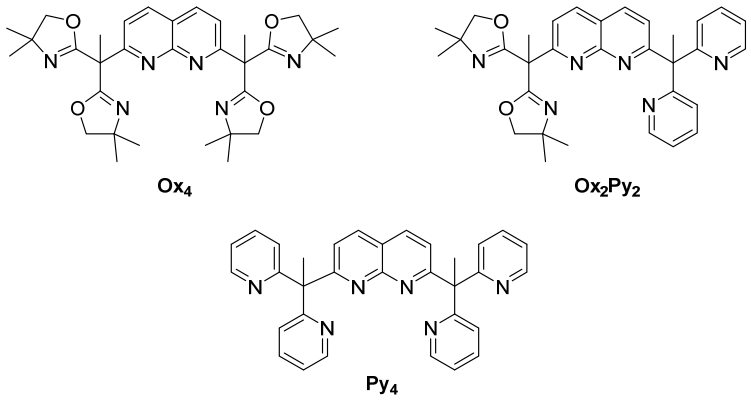

Scheme 2. Ligands used in this work.

With this background, in this study, we describe two novel naphthyridine-bridged ligands (Scheme 2) using bis-oxazoline moieties as binding site. Bis-oxazoline (BOX) ligands have found numerous applications, in particular in the field of asymmetric synthesis [20]. In particular, the steric bulk of the oxazoline group provides hindrance around the copper centers, stabilizing potential intermediates formed. This concept was applied by Meyer et al. in the copper–O_2 activation field showing that such an entity was able to stabilize a μ-η^2:η^2-peroxido-dicopper(II) complex [21].

Here, we have employed **Ox_4** and **Ox_2Py_2** ligands for the preparation of dinuclear copper(I) and (II) complexes. Aiming at generating mixed valent $Cu^{II}Cu^{III}$–oxygen species, we have followed two strategies. In a first approach (Strategy 1, Scheme 3), $Cu^{I}{}_2$ complexes have been reacted with O_2 in order to generate stable (μ-η^2:η^2) peroxido $Cu^{II}{}_2$ complexes that can be further reduced/protonated. The second approach (Strategy 2) is based on the electrochemical/chemical mono-oxidation of stable $Cu^{II}{}_2$-hydroxido or $Cu^{II}{}_2$-bis(μ-hydroxido) complexes, as previously developed by our group with the **Py_4** ligand [17].

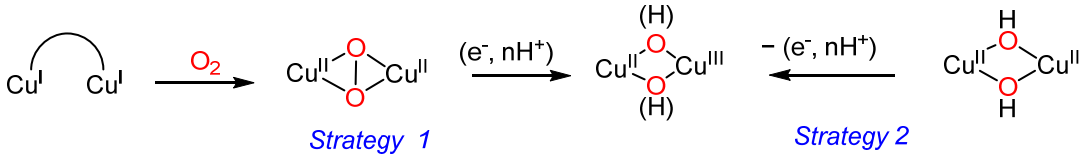

Scheme 3. Possible strategies for formation of $Cu^{II}Cu^{III}$ oxygen–mixed-valent species.

2. Results and Discussion

2.1. Ligands Synthesis

As shown in Scheme 2, the new ligands **Ox$_4$** and **Ox$_2$Py$_2$** display a common 1,8-naphthyridine spacer, the bis-oxazoline (BOX) or pyridine moieties (Py = 2,2′-dipyridylethane) serving as binding pockets (Scheme 2). The bis-oxazoline [22] and the pyridine (Py) [23] entities were synthesized according to procedures described in the literature. **Ox$_4$** was synthesized via lithiation of bis-oxazoline and subsequent reaction with the 2,7-dichloro-1,8-naphthyridine building block (synthesized according to literature procedures, in three steps) [24,25] with 20% yield. The ligand **Ox$_2$Py$_2$** was obtained in the same manner after two successive lithiations with 60% yield (Scheme 4). Corresponding ^{1}H (Figure S1) and ^{13}C (Figure S2) NMR are depicted in the Supplementary Materials along with ESI-MS spectra (Figure S3).

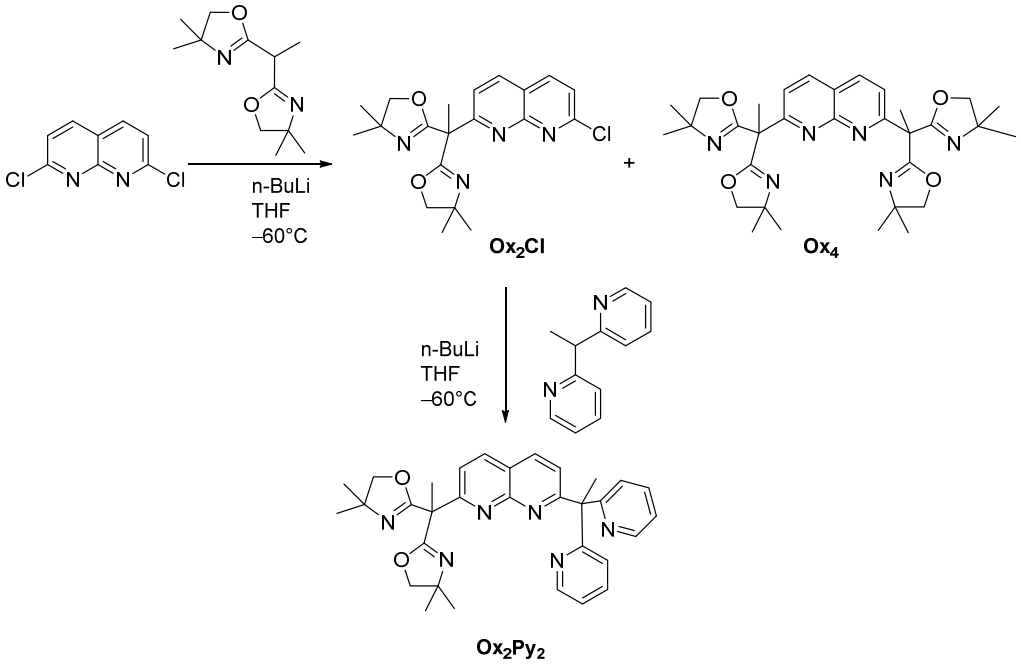

Scheme 4. Synthetic pathway for the ligands **Ox$_4$** and **Ox$_2$Py$_2$**.

2.2. Dicopper(I) Complexes

2.2.1. Synthesis and Characterizations

Complex **Cu$^I_2$Py$_4$** was synthesized according to the procedure described by Tilley et al. [26]. The two air-sensitive Cu(I) complexes based on **Ox$_4$** and **Ox$_2$Py$_2$** ligands (named **Cu$^I_2$Ox$_4$** and **Cu$^I_2$Ox$_2$Py$_2$**, respectively) were prepared using a similar procedure: under argon, one equivalent of ligand (**Ox$_4$** or **Ox$_2$Py$_2$**) was reacted with 2.1 equivalents of $[Cu^I(CH_3CN)_4]OTf$ in tetrahydrofuran (THF). In both cases, the reaction produced an orange precipitate with 70% or 92% yield, respectively. Unfortunately, no suitable crystal for X-ray diffraction analysis could be obtained. ^{1}H-NMR characterization of the two complexes was carried out in CD_3CN (Figure S4). Peaks centered around 4.0 ppm and 1.35 ppm can be attributed to the CH_2 and CH_3 groups of the oxazoline entities. Two peaks (doublets) were detected around 4 ppm, which did not appear on the ^{1}H-NMR spectrum of

the ligand itself. This result is a good indicator for copper(I) coordination to the ligand, as the two diastereotopic protons of the ligand are no longer in an equivalent environment. Two singlets at around 1.35 ppm matching to the CH_3 groups of the oxazoline moieties support this result.

2.2.2. Reactivity

In order to generate Cu_2/O_2 adducts, dioxygen was bubbled through solutions of $\mathbf{Cu^I_2Ox_4}$ and $\mathbf{Cu^I_2Ox_2Py_2}$ complexes in acetone at low temperature (T = 193 K). The reaction was monitored via UV-Vis spectroscopy (Figures 1 and S5). For both complexes, the spectrum of the initial dicopper(I) solution under N_2 was taken as the baseline for more accurate determination of the wavelength of the arising new absorption bands.

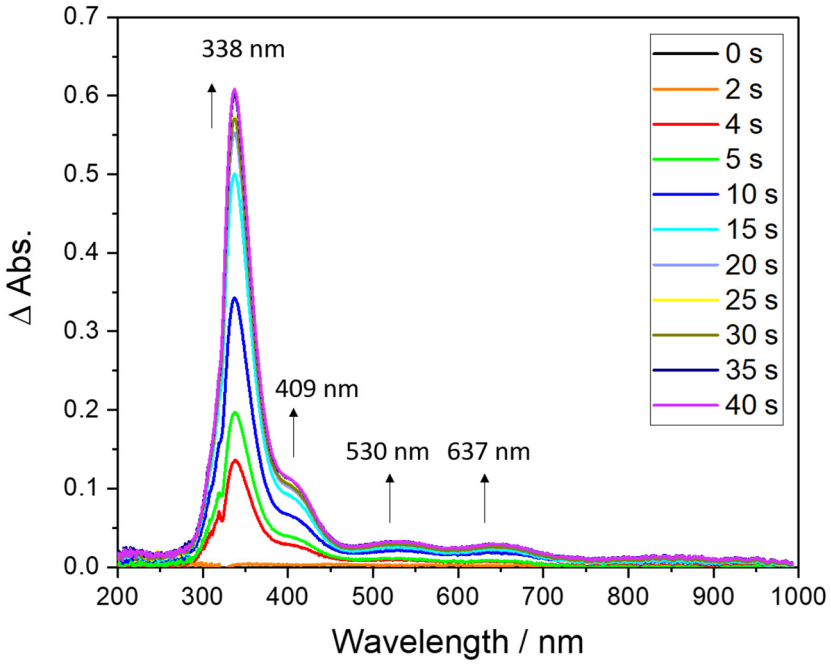

Figure 1. UV-vis monitoring of the addition of O_2 on $\mathbf{Cu^I_2Ox_4}$; parameters: optical path = 1 cm; solvent: acetone, concentration 0.094 mM, T = 193 K. The baseline was taken on the dicopper(I) complex solution before O_2 addition for better monitoring of the peroxide absorption bands (justifying the use of relative absorbance (ΔAbs.) instead of absorbance (Abs.) on the graph).

For complex $\mathbf{Cu^I_2Ox_4}$, four new bands with wavelengths ranging between 330 and 700 nm appeared rapidly upon addition of dioxygen. In particular, an intense absorption band at λ_{max} = 338 nm ($\varepsilon \approx 6400\ M^{-1}{\cdot}cm^{-1}$) together with a less intense one at λ_{max} = 409 nm ($\varepsilon \approx 1000\ M^{-1}{\cdot}cm^{-1}$) were observed. In addition, two low-intensity bands at 530 nm ($\varepsilon \approx 350\ M^{-1}{\cdot}cm^{-1}$) and 637 nm ($\varepsilon \approx 312\ M^{-1}{\cdot}cm^{-1}$) were detected. These absorptions correspond to low energy d–d transition, as reported in a parent dicopper complex [27]. The main absorption band at 338 nm is in the typical range of μ-η^2:η^2-peroxido-Cu^{II}_2 oxygen species and attributed to ligand-to-metal charge transfer (LMCT) from the peroxido to the copper centers [3]. A similar behavior was obtained with $\mathbf{Cu^I_2Ox_2Py_2}$. Indeed, a new absorption band was observed at λ_{max} = 367 nm upon addition of dioxygen ($\varepsilon \approx 2400\ M^{-1}{\cdot}cm^{-1}$) [3,28] (Figure S5). As for $\mathbf{Cu^I_2Ox_4}$, this wavelength value suggests the formation of side-on peroxido dicopper(II) species. However, both $\mathbf{Ox_4}$ and $\mathbf{Ox_2Py_2}$-based peroxides were shown to be poorly stable, hence excluding any further reduction/protonation for generating mixed-valent species such as shown in Scheme 3.

The reactivity of these μ-η^2:η^2-peroxido-Cu^{II}_2 oxygen adducts towards exogeneous substrates was then examined in acetone. Aromatic hydroxylation reactivity is well-known for dicopper(II)-μ-η^2:η^2-peroxido species, whereas dicopper(III)-bis-μ-oxido species are

better for electrophilic reactivity mechanisms such as hydrogen atom abstraction [28–31]. For both species generated here, no reactivity towards PPh_3 or benzaldehyde was observed. In contrast, with sodium 2,4-di-butylphenolate as substrate, both dicopper(II)-μ-η^2:η^2-peroxido gave rise to the carbon–carbon coupling product detected via GCMS (Figure S6) over arene oxygenation. These results are in line with those of Meyer et al. [21] using a bis-oxazoline derivatives. As previously suggested, the presence of the dimethyl bulky groups on oxazoline units impacts the reactivity by limiting the access of substrates to the Cu_2O_2 core.

2.3. Dicopper(II) Complexes

2.3.1. Synthesis and Characterizations

The next step consisted in exploring the redox properties of the dicopper(II) bis(μ-OH) **Ox_4** and **Ox_2Py_2** complexes. For this purpose, the complexation reactions of the two ligands were carried out in a classical manner. One equivalent of the ligand was dissolved in THF, and 2.1 equivalents of triethylamine and water (10 equivalents) were added followed by 2.1 equivalents of $Cu(OTf)_2$. Upon diffusion of di-isopropyl ether into a concentrated acetonitrile solution of complexes, single crystals for X-ray diffraction analysis were obtained with 71% and 75% yield, respectively. Details for X-ray analysis are in Table 1. Complex **1** (**$Cu^{II}_2Ox_4$**) crystallizes as a dinuclear complex with the Cu atoms bridged by two hydroxido groups (Figure 2a) with Cu–O–Cu angles close to 90.4°. The Cu1 and Cu2 copper atoms are set at a short distance from each other (2.7537(5) Å). The geometries of both copper atoms are described as a square-based pyramid (τ = 0.07 for Cu1 and 0.08 for Cu2) [32] with N1 and N2 of the naphthyridine spacer occupying the axial position. Although the equatorial distances are in the range of the values obtained for parent/relevant dinuclear complexes (1.9–2.1 Å) [17,33–35], the nitrogen of the naphthyridine is located at 2.43–2.46 Å from the copper(II) centers. These significantly longer distances could indicate a weaker donating group and a possible unbinding of these atoms in solution.

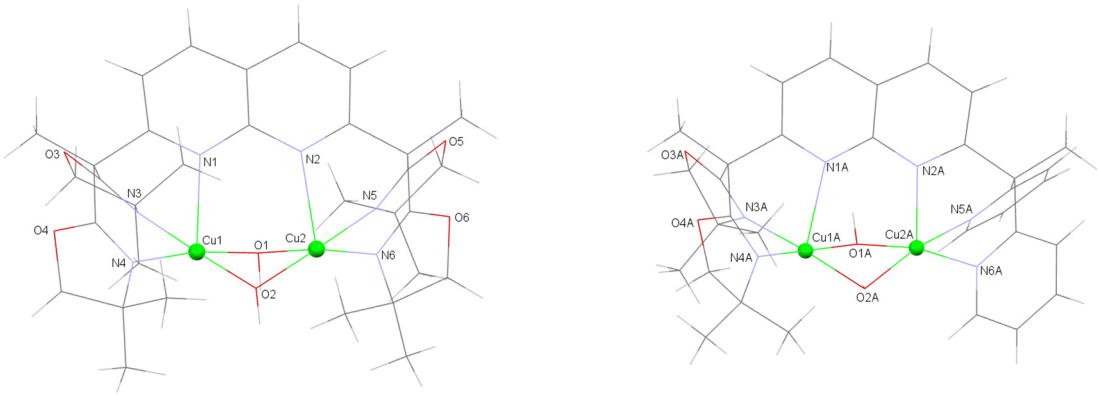

(**a**) (**b**)

Figure 2. Representation of cationic units of (**a**) $[(Cu_2(Ox_4))(\mu\text{-}OH)_2](CF_3SO_3)_2$ (**1**) and (**b**) $[(Cu_2(Ox_2Py_2)(\mu\text{-}OH)_2](CF_3SO_3)_2$ (**2A**). Selected bond lengths (Å) and angles (°) are reported in ESI (Tables S1 and S2). Others view and complete representation including counterions and solvent are in ESI (Figure S7a,b).

The similarly complexation of ligand **Ox_2Py_2** afforded compound **2** (**$Cu^{II}_2Ox_2Py_2$**) as a crystalline material. The unit cell encloses two crystallographically independent $[C_{32}H_{44}Cu_2N_6O_6](CF_3SO_3)_2$ entities and one CH_3CN as solvate. Each cationic unit displays two triflate counterions. Unit **2A** is shown in Figure 2b (other views on Figure S7b) and unit **2B** is shown in Figure S7c (Supporting Information); each consists of two copper atoms bridged by two hydroxido groups. Selected bond lengths and angles are reported in Tables S1 and S2 in the Supplementary Materials and display no significant difference between **2A** and **2B** dimers. In **2A**, the Cu1A-Cu2A distance is short (2.80) Å but rather long compared

to $\mathbf{Cu^{II}_2Py_4}$ (complex **3**) [17] and to $\mathbf{Cu^{II}_2Ox_4}$, with a distance of 2.75 Å. Each copper atom has a square-based pyramid geometry (τ = 0.01 for Cu1A and 0.02 for Cu2A) [32] with the equatorial positions occupied by the hydroxido groups and the nitrogen atoms of either the pyridines or the BOX entities and the axial positions occupied by the N atoms of the naphthyridine spacer. Bond distances between the Cu atoms and equatorial positions are of 1.9–2.0 Å. The axial bonds are longer at 2.47 Å for Cu1A-N1 (the side of the BOX units) and 2.26 Å for Cu2A-N2 (the side of the pyridine units).

UV-Vis characterization of the dicopper(II) complexes **1** and **2** was carried out in acetonitrile. The complexes exhibited intense electronic transitions in the UV region at 260, 305, 310 and 317 nm ($\varepsilon \sim 10\,000\ M^{-1}\ cm^{-1}$). These bands are similar to those of $\mathbf{Ox_4}$ and $\mathbf{Ox_2Py_2}$ free ligands and have been assigned as π–π^* transitions. Large bands at 580 nm and 570 nm, respectively, with weak values of molar absorptivity ($\varepsilon \sim 100\ M^{-1}\ cm^{-1}$) were observed for each complex and correspond to d–d transitions. These two complexes were also analyzed via ESI-MS in acetonitrile (Figure S8). Peaks were detected at 883 and 843 m/z corresponding to $[M\text{-}OTf]^+$ for $[(Cu_2(\mathbf{Ox_4}))(\mu\text{-}OH)_2](CF_3SO_3)_2$ and $[(Cu_2(\mathbf{Ox_2Py_2}))(\mu\text{-}OH)_2](CF_3SO_3)_2$, respectively, where M corresponds to the complex. Theoretical isotopic profiles matched experimental ones indicating that the complexes remain dinuclear in solution.

2.3.2. Electrochemical Oxidation of Complexes **1** and **2**

We further investigated the oxidation process for both dicopper(II) complexes **1** and **2**. Attempts to generate a mixed-valent $Cu^{II}Cu^{III}$ species were carried out via cyclic voltammetry (CV) in a CH_3CN solution with tetra-n-butyl ammonium perchlorate (TBAP) as the supporting electrolyte.

As shown in Figure 3, the two complexes displayed a reversible oxidation system at $E_{1/2}$ = 1.27 V and 1.09 V vs. Fc^+/Fc, respectively, for **1** and **2** at v = 100 $mV{\cdot}s^{-1}$ rendering them all out of reach of commonly used chemical oxidants [17]. Noteworthy, complex **1** showed a complete loss of reversibility at a lower scan rate (v = 20 $mV{\cdot}s^{-1}$) (Figure 3a), contrary to complex **2,** for which reversibility was still observed at v = 5 $mV{\cdot}s^{-1}$ (Figure 3b). Plots of the normalized anodic peak current $Iv^{-1/2}$ against the scan rate (v) (Figure S9) showed a particular increase of $Iv^{-1/2}$ at low scan rates for **1**. This result is indicative of an ECE mechanism (E = electrochemical and C = chemical) where the oxidation of the complex is followed by a chemical reaction on the experimental time scale, producing new species, which, in turn, can be oxidized. The oxidation of both complexes therefore involves, at room temperature, the formation of a transient species that has a half-life of several seconds. For the oxidation process of each complex, the number of electrons was determined by using the Randles–Sevcik equation [36,37] for scan rate values for which the system remained reversible. I_P was plotted against $v^{1/2}$ for complexes **1** and **2** (Figure S10), yielding values of n = 1.3 and 1.2, respectively, thus indicating a one-electron transfer for both complexes. This behavior is reminiscent of that previously obtained with complex **3** ($\mathbf{Cu^{II}_2Py_4}$), which displayed a reversible system at 1.26 V vs. Fc^+/Fc in the same conditions [17].

In order to avoid decomposition at room temperature because of the occurrence of an ECE process, the mono-electronic oxidized species were generated at −40 °C via bulk electrolysis of **1** and **2** (0.7 mM) in a 0.1 M NBu_4ClO_4/acetonitrile solution to the potentials of 1.41 V vs. Fc^+/Fc for **1** and 1.26 V vs. Fc^+/Fc for **2**. Bulk oxidation was accompanied by a color change from pale blue/colorless to yellow for complex **2** and colorless to brown for complex **1**. During the course of the low-temperature electrolysis, the samples were taken out and immediately frozen in liquid nitrogen for EPR analysis. For control experiments, to get the EPR spectrum of the final product, the oxidized species was also warmed to room temperature and then frozen in liquid nitrogen. Before electrolysis, the two complexes were EPR-silent (CH_3CN, 100 K). The EPR spectrum of complex **2** after oxidation via electrolysis is displayed in Figure 4, along with the spectrum of the product warmed to room temperature. Spectra were recorded at 15 K, but the same features were observed from 15 to 100 K. The oxidized complex displayed four clear lines (Figure 4) with coupling constant $A_{\|}$ of 173 G, the expected EPR spectrum for a mononuclear Cu^{II}

complex in an axial geometry (an unpaired electron coupling to the nuclear spin of one copper with $I = 3/2$). This is consistent with a valence-localized $Cu^{II}Cu^{III}$ species (the Cu^{III} being EPR silent), defined in the Robin Day classification system [38] as a class I (classes II and III represents slight and significant delocalization, respectively). The spectrum of the complex **1** after oxidation was less resolved but four lines were still observable ($A_{\|}$ = 177 G) (Figure S11). The loss of resolution of the signal from this oxidized complex could be due to more instability of the one-oxidized species that can also be stated by its lower reversibility of the CV (Figure 3a) at room temperature compared to complex **2** (Figure 3b). For the mono-oxidized species **1**, **2** and **3,** in all three cases, the EPR parameters of the spectra (see Figures 4 and S11) obtained after simulation show a Cu^{II} in an axial geometry [17]. It is therefore obvious that mono-oxidation of the complexes $\mathbf{Cu^{II}_2Ox_2Py_2}$ and $\mathbf{Cu^{II}_2Ox_4}$ leads to the formation of mixed-valent $Cu^{II}Cu^{III}$ species. After the oxidized samples had been warmed to room temperature, the recorded spectra of all complexes at 15K displayed broad signals, indicating a mixture of several Cu^{II} complexes in solution.

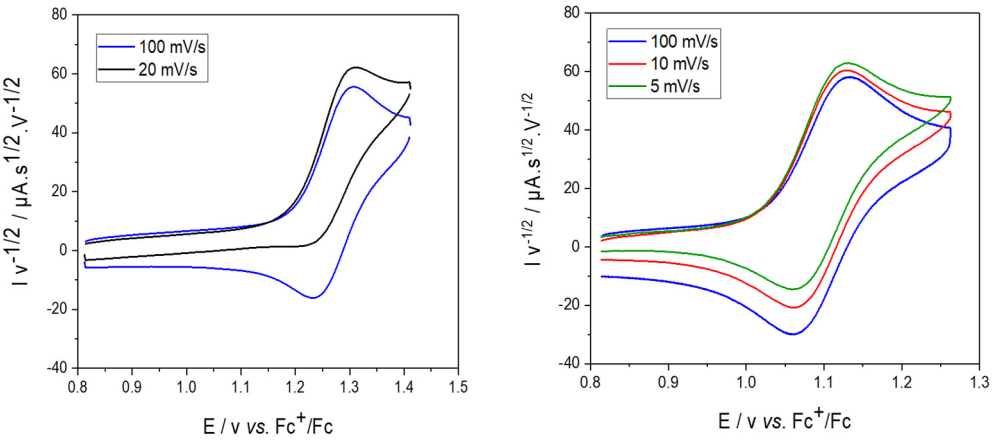

(**a**) (**b**)

Figure 3. Scan−rate−normalized CV for (**a**) complex **1** and (**b**) complex **2** (for each at 1 mM) in acetonitrile with 0.1 M NBu_4ClO_4; room temperature; scan rates 100 $mV{\cdot}s^{-1}$ (blue), 20 $mV{\cdot}s^{-1}$ (black), 10 $mV{\cdot}s^{-1}$ (red) and 5 $mV{\cdot}s^{-1}$ (green).

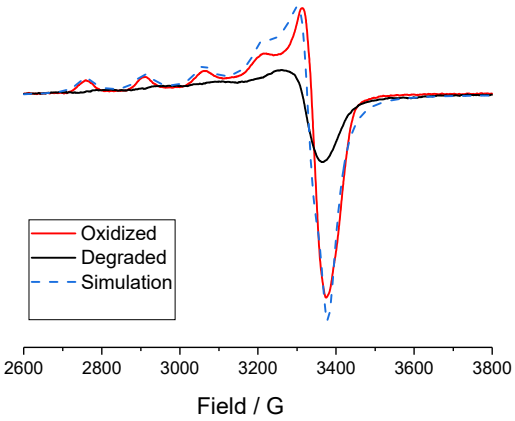

Figure 4. EPR spectra of complex **2** after oxidation after bulk electrolysis at −40 °C (red), and after warming to room temperature (black) in frozen solution (0.1 M NBu_4ClO_4 in acetonitrile) of 0.7 mM of **2** recorded at 15 K; frequency = 9.419 GHz. Simulation was carried out with the EasySpin program [39] assuming the following parameter: $g_{\perp}$ = 2.065, $g_{//}$ = 2.307, $A_{\perp}$ = 0 G, $A_{//}$ = 173 G.

UV-Vis-NIR time-resolved spectroelectrochemistry experiments were carried out at room temperature to further characterize the unstable mono-oxidized species. Upon mono-

oxidation of $\mathbf{Cu^{II}_2Ox_4}$ (**1**), new absorption bands were detected at λ_{max} = 380 nm, 480 nm (both $\varepsilon \approx 735\ M^{-1}{\cdot}cm^{-1}$) and 630 nm (weak) (Figure S12). In the NIR region, a very low-intensity and broad band centered at 1680 nm was observed (Figure S12). For this complex, the redox process was found to be irreversible at the defined scan rate ($30\ mV{\cdot}s^{-1}$), suggesting a fast evolution of the generated mixed-valent species.

For $\mathbf{Cu^{II}Ox_2Py_2}$ **(2)**, spectroelectrochemical measurements displayed slightly different features than for **1**. New absorption bands were detected at λ_{max} = 360 nm ($3420\ M^{-1}{\cdot}cm^{-1}$) and 424 nm (sh, $2140\ M^{-1}{\cdot}cm^{-1}$) (Figures 5 and S13). In the near infrared region, a broad and weak band appeared at λ_{max} = 1185 nm ($120\ M^{-1}{\cdot}cm^{-1}$) (Figure S13). The process was found to be fully reversible as shown by CV and from spectroscopic data since these absorption bands disappeared upon back reduction. Aiming at better analyzing the oxidized product from **2**, we determined the bandwidth at half-height ($\Delta\tilde{\nu}_{1/2}$ = 2460 cm^{-1}) by fitting the NIR experimental curve (Figure S14). From this value and by assuming a Cu−Cu distance of 2.80 Å from the X-ray structure of **2**, we determined the electronic coupling matrix element H_{ab} (determined from the Mulliken-Hush expression [40,41]) as well as the ratio between the experimental and theoretical values of $\Delta\tilde{\nu}_{1/2}$ (Γ parameter). The calculations yielded H_{ab} = 373 cm^{-1} and Γ = 0.45, as typically found for a class II system in the Robin−Day classification, i.e., low delocalization of the charge, here at room temperature. Noteworthy, this result is close to that obtained with $\mathbf{Cu^{II}Py_4}$ (**3**) (H_{ab} = 322 cm^{-1} and Γ = 0.39) [17] and demonstrates the strong similarities between $\mathbf{Cu^{II}Ox_2Py_2}$ and $\mathbf{Cu^{II}Py_4}$ complexes. It likely suggests that the oxidation occurs on the copper/pyridine moieties for complex **2**.

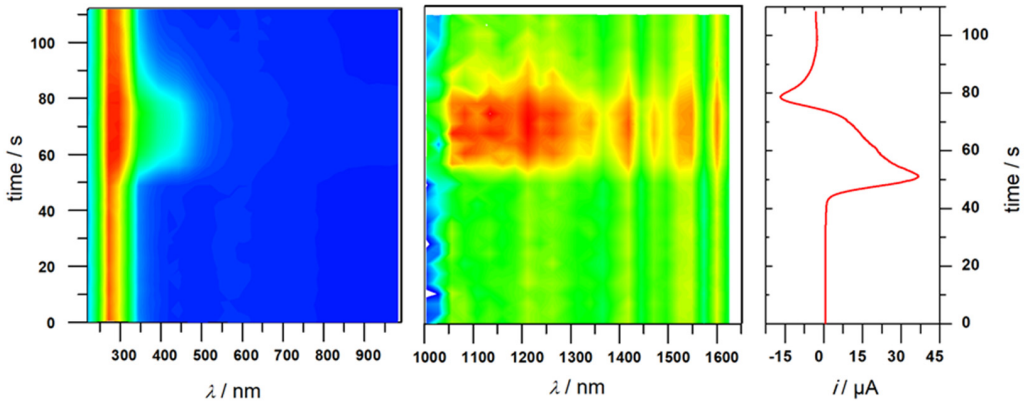

Figure 5. UV-Vis−NIR monitoring of the oxidation of complex **2** via spectroelectrochemistry showing the reversibility of the redox process. Right: current intensity variation with time taken from the CV at $v = 30\ mV{\cdot}s^{-1}$. Conditions: 7 mM in 0.1 M NBu_4ClO_4 in acetonitrile, optical path = 0.2 mm, working electrode: Pt, room temperature.

In regard to the observed reactivity toward toluene (bond dissociation energy (BDE) = 89.8 kcal mol^{-1}) [42] of $Cu^{II}Cu^{III}$ species generated electrochemically from $\mathbf{Cu^{II}_2Py_4}$, the reactivity of the mono oxidized species from **1** and **2** were probed via CV with (over 100 equiv.) and without toluene. For both complexes, the CV remained the same when toluene was added, suggesting no reactivity between the $Cu^{II}Cu^{III}$ species and toluene at this timescale. Few $Cu^{II}Cu^{III}$ species are reported in the literature [17,33–35] and besides our previous studies [18], only one result demonstrated a reactivity on dihydroanthracene [33], a rather weak C-H bond.

To test a possible reason of this lack of observed reactivity, the ligands were analyzed after the monoelectronic-oxidation of the complexes (0.7 mM) through exhaustive electrolysis in NBu_4ClO_4/CH_3CN at −40 °C at 1.26 V vs. Fc^+/Fc for complex $\mathbf{Cu^{II}_2Ox_2Py_2}$ and at 1.41 V vs. Fc^+/Fc for complex $\mathbf{Cu^{II}_2Ox_4}$ under air. After electrolysis, the solutions were warmed to room temperature.

For identification of the oxidation products, the demetallation residue was analyzed via ESI mass spectrometry (Figures S15 and S16). In the case of $\mathbf{Cu^{II}_2Ox_4}$, the protonated ligand $[LH + H]^+$ (where LH represent the ligand) was observed at 575 m/z, but peaks at 591 m/z, 613 m/z and 629 m/z indicated the ligand hydroxylation as $[LOH + H]^+$, $[LOH + Na]^+$ and $[LOH + K]^+$, respectively, corresponding to the addition of an O atom. This behavior is consistent with change of the $C(CH_3)_2$ into $C(CH_3)(CH_2OH)$ as depicted in Figure S17. The peak at 630 m/z was tentatively attributed to $[LCHOHCN + H]^+$, which could be formed by a radical coupling of the oxazoline unit with the CH_3CN solvent. Similar products were observed from the residue of $\mathbf{Cu^{II}_2Ox_2Py_2}$: peaks at 535 m/z and 557 m/z from the ligand $[LH + H]^+$, $[LH + Na]^+$, respectively, and peaks at 551 m/z and 573 m/z from the hydroxylated product $[LOH + H]^+$ and $[LOH + Na]^+$. Peaks at 590 m/z and 612 m/z could tentatively be assigned to products $[LCHOHCN + H]^+$ and $[LCHOHCN + Na]^+$, respectively. All products are consistent with a proton coupled electron transfer as the initial step of the reaction. The oxidation of the relatively strong C-H bonds of the ligands is not surprising given the high oxidation potential of the complexes (where the oxidation potential and the pKa are the two thermodynamic driving forces for proton coupled electron transfers) [42].

From the non-electrolyzed complexes (but using the same treatment with concentrated KOH), no hydroxylated products or peaks assigned to the formation of LCHOHCN were observed on the residues, demonstrating that the changes to the ligand are linked to the generation of the $Cu^{II}Cu^{III}$ species.

3. Materials and Methods

3.1. General

Reagents were purchased from commercial sources and were used without purification. The solvents were purified via standard methods before use. ESI mass spectra were recorded on an Esquire 3000 plus Bruker Daltonis with nanospray inlet. UV-Vis analyses were performed using a Cary 50 spectrophotometer operating in the 200–1000 nm range with quartz cells. The temperature was maintained at 25 °C with a temperature control unit. NMR solution spectra (^1H and ^{13}C) at 298 K were recorded on a unity Plus 400 MHz Varian spectrometer with the deuterated solvent as a lock. X-band EPR spectra were recorded in a range of 15–100 K with a Bruker EMX Plus spectrometer equipped with a nitrogen flow (or He flow) cryostat and operating at 9.4 GHz (X band). All spectra presented were recorded under non-saturating conditions. Simulation of EPR spectra was carried out with EasySpin program [39]. All electrochemical measurements were carried out under an argon atmosphere at room temperature using a Biologic SP-300 instrument. Experiments were performed with solutions of the complexes containing 0.1 M of the supporting electrolyte ($TBA{\cdot}ClO_4$). For cyclic voltammetry, a standard three-electrode configuration was used consisting of a glassy carbon (d = 3 mm) working electrode, a platinum counter electrode and an Ag wire placed in an $AgNO_3$ (0.01 M in CH_3CN)/NBu_4ClO_4 (0.1 M in CH_3CN)) solution as a pseudo reference electrode. The system was systematically calibrated against ferrocene after each experiment and all the potentials are therefore given versus the Fc^+/Fc redox potential. Low-temperature electrolysis was carried out with a home-designed 3-electrode cell (WE: Carbon felt, RE: Pt wire, CE: Pt grid) dipped in an acetone/dry ice bath at −40 °C for 45 min. Samples for EPR and UV-Vis analysis of the mixed-valent complex were taken every 15 min. They were instantly frozen in liquid nitrogen for EPR measurements.

3.2. Ligands' Syntheses

Synthesis of ligand Ox_4. According to the literature procedures [22,24], the intermediates 2,7-dichloro-1,8-naphthyridine and BOX were synthesized. A total of 1.25 g (5.56×10^{-3} mol, 2.2 eq) of BOX dissolved in 40 mL of freshly distilled THF under argon and cooled to –60 °C was slowly added to 2.5 mL (5.56×10^{-3} mol, 2.2 eq) of 2.4 M n-BuLi. The colorless solution was stirred for 30 min and 0.526 g of 2,7-dichloro-1,8-naphthyridine was added, leading to a beige precipitate in a red-orange solution. The solution was stirred

overnight and reached room temperature, resulting in the solubilization of the precipitate. After addition of water (5 mL), THF was evaporated and a 40 mL of water was added. The solution was extracted with dichloromethane (DCM) and dried over Na_2SO_4. The residue was purified via column chromatography (gradient of acetone/pentane) over silica to give products Ox_2Cl and Ox_4 (79% and 20%, respectively). ^{1}H-NMR (400 MHz, CD_3CN), δ_H (ppm): 8.27 (2H, d, *J* = 8.8 Hz, C_4H), 7.70 (2H, d, *J* = 8.8 Hz, C_3H), 3.97 (8H, s, $C_{10}H$), 1.95 (6H, s, C_7H), 1.23 (24H, s, $C_{11}H$); ^{1}H-NMR (400 MHz, $CDCl_3$), δ_H (ppm): 8.07 (2H, d, *J* = 8.8 Hz, C_4H), 7.66 (2H, d, *J* = 8.4 Hz, C_3H), 4.00 (8H, s, $C_{10}H$), 2.09 (6H, s, C_7H), 1.32 (24H, s, $C_{11}H$); ^{13}C-NMR (101 MHz, $CDCl_3$), δ_C (ppm): 165.44 (C_6), 162.71 (C_2), 154.16 (C_8), 136.10 (C_4), 122.14 (C_3), 120.66 (C_5), 79.47 (C_{10}), 67.36 (C_9), 50.58 (C_1), 27.93 (C_{11}), 23.15 (C_7); ESI-MS: m/z 575.4 $[M + H]^+$; elemental analysis: $C_{36}H_{42}N_6O_4 \cdot 1.75(H_2O)$. Theoretical (%): C: 63.40, H: 7.57 and N: 13.86. Obtained: C: 63.37, H: 7.24 and N: 13.77.

Synthesis of ligand Ox_2Py_2. In total, 0.70 g (0.38×10^{-3} mol, 1.1 eq) of 1,1-di-(2-pyridyl)ethane [23] was dissolved in 15 mL of freshly distilled THF under argon and cooled to −50 °C, followed by the slow addition of 0.26 mL (0.38×10^{-3} mol, 1.1 eq) of 1.4 M n-BuLi and the red solution was stirred for 30 min. Then, 0.133 g of 2,7-dichloro-1,8-naphthyridine was added using a powder finger. The solution was stirred overnight and allowed to reach room temperature, resulting in the formation of a precipitate. Then, 1 mL of water (1 mL) was added, dissolving the precipitate; the THF evaporated and water (20 mL) was added, and the solution was extracted with DCM (4×15 mL) and dried over $MgSO_4$. The residue was purified via column chromatography (gradient of acetone/pentane) over silica to give the ligand Ox_2Py_2 (140 mg, 76%). ^{1}H-NMR (400 MHz, CD_3CN), δ_H (ppm): 8.48 (2H, d, *J* = 4.4 Hz, $C_{16}H$), 8.22 (1H, d, *J* = 8.4 Hz, C_7H), 8.15 (1H, d, *J* = 8.4 Hz, C_4H), 7.67 (1H, d, *J* = 8.4 Hz, C_8H), 7.66 (2H, dt, J_1 = 8.0 Hz, J_2 = 2.0 Hz, $C_{14}H$), 7.40 (1H, d, *J* = 8.8 Hz, C_3H), 7.23 (2H, d, *J* = 8.0 Hz, $C_{13}H$), 7.20 (2H, dd, J_1 = 7.6 Hz, J_2 = 4.9 Hz, $C_{15}H$), 3.95 (4H, s, $C_{19}H$), 2.35 (3H, s, $C_{11}H$), 1.93 (3H, s, $C_{21}H$), 1.21 (12H, s, $C_{20}H$); ^{13}C-NMR (101 MHz, CD_3CN), δ_C (ppm): 170.72 (C_6), 166.57 (C_2), 166.21 (C_9), 163.50 (C_{17}), 154.85 (C_{12}), 149.47 (C_{16}), 137.65 (C_4), 137.24 (C_{14}), 136.99 (C_7), 124.79 (C_3), 124.56 (C_{13}), 123.14 (C_8), 122.60 (C_{15}), 121.00 (C_5), 80.09 (C_{19}), 68.20 (C_{18}), 62.02 (C_{10}), 51.41 (C_1), 30.69 (C_{11}), 28.16 (C_{20}), 27.80 (C), 26.27 (C), 23.06 (C_{21}); ESI-MS: m/z 557 $[M + Na]^+$, 535 $[M + H]^+$; elemental analysis: $C_{32}H_{34}N_6O_2 \cdot 0.6(CH_2Cl_2)$. Theoretical: C: 66.86, H: 6.06 and N: 14.35. Obtained: C: 66.91, H: 6.27 and N: 14.08.

3.3. Complexes Syntheses

Synthesis of complex $Cu^I_2Ox_2Py_2$. In a glove box, the ligand Ox_2Py_2 (0.073 g, 1.4×10^{-4} mol, 1 eq) was dissolved in 4 mL of distilled THF and added to a solution of $[Cu^I(CH_3CN)_4]OTf$ (0.11 g, 2.9×10^{-4} mol, 2.1 eq) in 10 mL of THF. The resulting suspension was stirred for 12 h and then filtered. The solid was recovered and dried under vacuum giving a bright orange solid (0.127 g, 92%). ^{1}H-NMR (400 MHz, CD_3CN), δ_H (ppm): 8.57 (2H, br, $C_{16}H$), 8.35 (2H, m, $C_{4\&7}H$), 7.90 (2H, m, $C_{3\&8}H$), 7.77 (2H, br, $C_{14}H$), 7.51 (2H, br, $C_{13}H$), 7.37 (2H, br, $C_{15}H$), 4.07 (2H, d, *J* = 8.2 Hz, $C_{19}H$), 3.90 (2H, d, *J* = 8.2 Hz, $C_{19}H$), 2.43 (3H, s, $C_{11}H$), 2.13 (3H, s, $C_{21}H$), 1.39 (6H, s, $C_{20}H$), 1.32 39 (6H, s, $C_{20}H$); elemental analysis: $C_{36}H_{37}Cu_2F_6N_7O_8S_2 \cdot 2(H_2O) \cdot 1.5(CH_3CN)$. Theoretical: C: 42.64, H: 4.17 and N: 10.84. Obtained: C: 42.32, H: 4.03 and N: 10.82.

Synthesis of complex$Cu^I_2Ox_4$. In a glove box, the ligand Ox_4 (0.041 g, 7.5×10^{-5} mol, 1 eq) was dissolved in 4 mL of distilled THF and added to a solution of $[Cu^I(CH_3CN)_4]OTf$ (0.057 g, 1.5×10^{-4} mol, 2.1 eq) in 10 mL of THF. The resulting suspension was stirred for 12 h, followed by filtering, and the solid was dried under vacuum, giving a bright orange solid (0.050 g, 70%). ^{1}H-NMR (400 MHz, CD_3CN), δ_H (ppm): 8.45 (2H, d, *J* = 8.4 Hz, C_4H), 7.61 (2H, *J* = 8.4 Hz, C_3H)), 4.10 (4H, *J* = 8.4 Hz, $C_{10}H$), 3.96 (4H, d, *J* = 8.4 Hz, $C_{10}H$), 2.08 (6H, s, C_7H), 1.40 (12H, s, $C_{11}H$), 1.36 (12H, s, $C_{11}H$); elemental analysis: $C_{36}H_{45}Cu_2F_6N_7O_{10}S_2 \cdot 3(H_2O) \cdot (CH_3CN) \cdot (CH_2Cl_2)$. Theoretical: C: 39.24, H: 4.70 and N: 9.51. Obtained: C: 39.16, H: 4.35 and N: 9.41.

Synthesis of the complex $[(Cu_2(Ox_4)(\mu\text{-}OH)_2](CF_3SO_3)_2$ (**1**). Briefly, 130 mg of the ligand Ox4 (2.2×10^{-4} mol, 1 eq) was dissolved in 10 mL of THF. Triethylamine (66 µL, 4.7×10^{-4} mol, 2.1 eq) was added, followed by a solution of $Cu(OTf)_2$ (170 mg, 4.6×10^{-4} mol, 2.1 eq) in 5 mL THF. A blue precipitate gradually formed, and after 3 h, the solution was decanted and the solid washed in THF. The blue solid was recrystallized via slow diffusion of DIPE into a solution of CH_3CN to give blue crystals (160 mg, 71%) suitable for X-ray diffraction. ESI (acetonitrile): m/z 883 $(M\text{-}OTf)^+$, 359 $(M\text{-}(OTf)_2)^{2+}$. UV-Vis (acetonitrile) λ/nm (ε/M^{-1} cm^{-1}): 253 (9700), 305 (8300), 310 (8600), 317 (10000) 580 (94). Elemental analysis: $C_{34}H_{46}Cu_2F_6N_6O_{13}S_2 \cdot H_2O$. Theoretical: C: 38.82, H: 4.41 and N: 7.99. Obtained: C: 38.85, H: 4.51 and N: 8.34.

Synthesis of the complex $[(Cu_2(Ox_2Py_2)(\mu\text{-}OH)_2](CF_3SO_3)_2$ (**2**). First, 50 mg of the ligand Ox_2Py_2 (9.4×10^{-5} mol, 1 eq) was dissolved in 5 mL of THF. H_2O (17 µL, 9.4×10^{-4} mol, 10 eq) and triethylamine (27 µL, 1.9×10^{-4} mol, 2.1 eq) were added, followed by a solution of $Cu(OTf)_2$ (71 mg, 2.0×10^{-4} mol, 2.1 eq) in 5 mL THF. A blue precipitate gradually formed, and after 3 h, the solution was decanted and the solid washed in THF. The blue solid was dissolved in 1 mL of CH_3CN, 40 mL of THF was added and the mixture placed in the freezer (−20 °C) for one week, after which crystals had formed. These were collected, and dried under vacuum (73 mg, 75%). X-ray diffraction quality crystals were obtained via slow diffusion of DIPE into a solution of CH_3CN. ESI (acetonitrile): m/z 843 $(M\text{-}OTf)^+$, 338 $(M\text{-}(OTf)_2\text{-}H_2O)^{2+}$. UV-Vis (acetonitrile) λ/nm (ε/M^{-1} cm^{-1}): 268 (8200), 303 (7400), 306 (8600), 317 (7300) 570 (100). Elemental analysis: $C_{34}H_{36}Cu_2F_6N_6O_{10}S_2 \cdot 0.5(H_2O)$. Theoretical: C: 40.72, H: 3.72 and N: 8.38. Obtained: C: 40.69, H: 3.60 and N: 8.58.

3.4. Crystallographic Studies

Crystals were mounted on a Kappa APEXII Bruker-Nonius diffractometer equipped with an Incoatec µsource with multilayer mirror mono-chromated Mo-Kα radiation (λ = 0.71073 Å) and a cryosystem Oxford cryostream cooler. Intensities were corrected for Lorentz and polarization (EVAL14) and for absorption (SADABS). Structural resolutions were carried out via direct method (SIR97) or the charge flipping method (Superflip) and refinement via full-matrix least squares on F2 (SHELX2013) [43] completed using the OLEX 2 analysis package [44]. The refinement of all non-hydrogen atoms was carried out with anisotropic thermal parameters. Hydrogen atoms were generated in idealized positions (excluding the hydroxido bridges, which were located on the difference Fourier map), riding on the carrier atoms, with isotropic thermal parameters. CCDC 2266887 and 2266888 contain the full data collection parameters and structural data for **2** and **1**, respectively.

Table 1. Crystallographic data for $[(Cu_2(Ox_4))](CF_3SO_3)_2$ (**1**) and $[(Cu_2(Ox_2Py_2)(\mu\text{-}OH)_2](CF_3SO_3)_2$ (**2**).

Compound	1	2
Chemical Formula	$[C_{32}H_{44}Cu_2N_6O_6](CF_3O_3S)_2$	$2[C_{32}H_{36}Cu_2N_6O_4)(CFO_3S)_2]\cdot CH_3CN$
Formula mass	1033.95	2028.83
Morphology	plate	plate
Color	blue	blue
Crystal size (mm)	0.48 × 0.3 × 0.1	0.45 × 0.2 × 0.1
Crystal system	monoclinic	triclinic
Space group	*P*1 21/*n* 1	*P*-1
a [Å]	10.332 (2)	12.377 (3)
b [Å]	30.427 (6)	14.361 (3)
c [Å]	13.415 (3)	23.657 (5)
α [°]	90	84.30 (3)
β [°]	92.80 (3)	82.98 (3)
γ [°]	90	83.00 (3)
Unit-cell volume [$Å^3$]	4212.2 (15)	4127.1 (15)
D_x ($g\cdot cm^{-3}$)	1.63	1.633

Table 1. *Cont.*

Compound	1	2
T [K]	200	200
Z	4	2
μ [mm^{-1}]	1.202	1.222
Total reflections	68,415	77,009
Unique reflections	12,173	18,827
Obsd. reflections	9889 ($F > 2\sigma$)	11,658 ($F > 2\sigma$)
Rint.	0.0501	0.0961
R^a	0.0400	0.0868
$R(w)^a$	0.0873	0.2176
Goodness of fit *S*	1.085	1.061
$\Delta\rho_{min}/\Delta\rho_{max}$ ($e{\cdot}Å^{-3}$)	−0.641/0.574	−1.310/1.754
CCDC Number	2,266,888	2,266,887

[a] Refinement based on F where $w = 1/[\sigma^2(Fo)^2 + (0.0288p)^2 + 5.5580\ p]$ with $p = (Fo^2 + 2Fc^2)/3$ for **1**, $w = 1/[\sigma^2(Fo)^2 + (0.1196p)^2 + 17.8205\ p]$ with $p = (Fo^2 + 2Fc^2)/3$ for **2**.

3.5. Spectroelectrochemistry

Thin layer room-temperature UV-Vis-NIR spectroelectrochemistry was carried out with a specific home-designed cell in a reflectance mode (WE: platinum, RE: Pt wire, CE: Pt wire). The UV-Vis and Vis-NIR optic fiber probes were purchased from Ocean Optics. Time-resolved UV-Vis-NIR detection was performed with QEPro and NIRQuest spectrometers (Ocean Insight, Orlando, FL, USA). Spectroscopic data were acquired using the Oceanview software. A DH-2000-BAL light source (Ocean Optics) was used for these experiments. The potential of the spectroelectrochemical cell was monitored using an AUTOLAB PGSTAT 100 (Metrohm, The Netherlands) potentiostat controlled by the NOVA 1.11 software.

4. Conclusions

Two new bridged ligands bearing a naphthyridine spacer and symmetrical or unsymmetrical coordination environment including a bis-oxazoline arm were successfully synthetized. The related Cu^I_2 complex with four pyridine arms (**Py$_4$**) [26] displayed no dioxygen activation, whereas the corresponding Cu_2^I complexes from **Ox$_2$Py$_2$** and **Ox$_4$** ligands were shown to bind dioxygen at −40 °C yielding μ-η^2:η^2-peroxido-Cu^{II}_2 species as clearly observed by using UV-Vis spectroscopy. For both, preliminary reactivity studies with sodium 2,4-di-*tert*-butylphenolate were performed. The resulting product (3,3′,5,5′-tetra-*tert*-butyl-2,2′-biphenol) indicated C-C coupling, whereas no *ortho*-hydroxylation was observed. The corresponding Cu^{II}_2 complexes **1** (**Cu$^{II}_2$Ox$_4$**) and **2** (**Cu$^{II}_2$Ox$_2$Py$_2$**) have been prepared and characterized via single-crystal X-ray diffraction. Electrochemical mono-oxidation provided access to mixed-valent $Cu_2^{II,III}$ *μ*-hydroxido species with charge localization on one of the two copper ions. ESI-MS of the solution after electrolysis and demetallation show unequivocal evidence of intramolecular oxidation of the ligand through the bis-oxazoline moieties, contrary to complex **3** (**Cu$^{II}_2$Py$_4$**), which is active in electrocatalysis at room temperature of exogenous substrate [18]. The present study therefore emphasizes that the electrochemically produced $Cu^{II}Cu^{III}$ species are competent for aliphatic oxidation of C-H bonds (intramolecular or external substrate). In order to further advances towards generating a catalytic system (or oxidation of an external substrate), efforts on the synthesis of more robust ligands are currently being pursued.

Supplementary Materials: The following supporting information can be downloaded at: https://www.mdpi.com/article/10.3390/inorganics11080332/s1, Figure S1: ^{1}H NMR spectra of ligand Ox_4 and Ox_2Py_2; Figure S2: ^{13}C NMR spectra of ligand Ox_4 and Ox_2Py_2; Figure S3: ESI-MS spectra of ligand Ox_4 and Ox_2Py_2; Figure S4: ^{1}H-NMR spectra of $Cu^{I}{}_2Ox_4$ and $Cu^{I}{}_2Ox_2Py_2$; Figure S5: UV-vis spectrum after addition of O_2 to the complex $Cu^{I}{}_2Ox_2Py_2$; Figure S6: GCMS of the resulting solution after reaction of the μ-η^2:η^2-peroxo-$Cu^{II}{}_2$ species from complex $Cu^{I}{}_2Ox_4$ with 2,4-di-*tert*-butylphenol, Figure S7: Molecular structure of **1**, **2A** and **2B**; Figure S8: ESI-MS spectra of complexes $Cu^{II}{}_2Ox_4$ (**1**) and $Cu^{II}{}_2Ox_2Py_2$ (**2**); Figure S9: Plots of the normalized peak current $Iv^{-1/2}$ against the scan rate v for complexes **1**, **2** and $[(Cu_2(Py_4))(\mu\text{-}OH)_2](CF_3SO_3)_2$; Figure S10: Plots of the I against $v^{1/2}$ for complexes **1**, **2** and $[(Cu_2(Py_4))(\mu\text{-}OH)_2](CF_3SO_3)_2$; Figure S11: EPR spectrum of the mono-oxidized complex **1** after bulk electrolysis at −40 °C, and after heating to room temperature; Figure S12: UV-Vis-NIR spectroelectrochemistry data of **1** (a) Time-monitoring of the oxidation process; (b) Selected UV-Vis and NIR spectra at different time intervals; (c) CV of the complex during the spectroelectrochemical measurement; Figure S13: UV-Vis-NIR spectroelectrochemistry data of compound **2**; (a) Selected UV-Vis and NIR spectra from the spectroelectrochemical at different time intervals; (b) CV of the complex during the spectroelectrochemical measurement; Figure S14: Experimental and simulated of the NIR band obtained by spectroelectrochemistry of compound **2**; Figure S15: ESI-MS spectrum of the complex $Cu^{II}{}_2Ox_4$ after electrolysis, demetallation and purification; Figure S16: ESI-MS spectrum of the complex $Cu^{II}{}_2Ox_4$ after electrolysis, demetallation and purification; Figure S17: Proposed mechanisms; Table S1: Selected bond distances [Å] in **1**, **2A** and **2B** from X-Ray data; Table S2: Selected angles [°] in **1**, **2A** and **2B** from X-ray data.

Author Contributions: Formal analysis, investigation, J.A.I., N.L.P. and A.T.-P.; resources, J.A.I., G.G., F.M. and C.P.; data curation, N.L.P. and C.B.; writing—original draft preparation, C.B. and A.T.-P.; writing—review and editing, N.L.P., C.B. and A.T.-P.; project administration, N.L.P., C.B. and A.T.-P.; funding acquisition, N.L.P., C.B. and A.T.-P. All authors have read and agreed to the published version of the manuscript.

Funding: This research was funded by ANR (The French research agency), grant number ANR-22-CE07-0032 (COSACH) and Labex ARCANE (ANR-11-LABX-0003-01).

Data Availability Statement: Data is contained within the article or Supplementary Materials.

Acknowledgments: The authors gratefully acknowledge The French research agency (ANR) for support (ANR-22-CE07-0032). The authors are grateful to ICMG UAR 2607 for the analytical facilities (NMR, ESI-MS, EPR and X-ray). This work has been partially supported by the CBH-EUR-GS (ANR-17-EURE-0003) program, in the framework of which this work was carried out.

Conflicts of Interest: The authors declare no conflict of interest.

References

1. Elwell, C.E.; Gagnon, N.L.; Neisen, B.D.; Dhar, D.; Spaeth, A.D.; Yee, G.M.; Tolman, W.B. Copper−Oxygen Complexes Revisited: Structures, Spectroscopy, and Reactivity. *Chem. Rev.* **2017**, *117*, 2059–2107. [CrossRef] [PubMed]
2. Quist, D.A.; Diaz, D.E.; Liu, J.J.; Karlin, K.D. Activation of Dioxygen by Copper Metalloproteins and Insights from Model Complexes. *J. Biol. Inorg. Chem.* **2017**, *22*, 253–288. [CrossRef] [PubMed]
3. Keown, W.; Gary, J.B.; Stack, T.D.P. High-Valent Copper in Biomimetic and Biological Oxidations. *J. Biol. Inorg. Chem.* **2017**, *22*, 289–305. [CrossRef] [PubMed]
4. Trammell, R.; Rajabimoghadam, K.; Garcia-Bosch, I. Copper-Promoted Functionalization of Organic Molecules: From Biologically Relevant Cu/O_2 Model Systems to Organometallic Transformations. *Chem. Rev.* **2019**, *119*, 2954–3031. [CrossRef]
5. Garcia-Bosch, I.; Cowley, R.E.; Díaz, D.E.; Peterson, R.L.; Solomon, E.I.; Karlin, K.D. Substrate and Lewis Acid Coordination Promote O–O Bond Cleavage of an Unreactive $L_2CuII_2(O_2{}^{2-})$ Species to Form $L_2CuIII_2(O)_2$ Cores with Enhanced Oxidative Reactivity. *J. Am. Chem. Soc.* **2017**, *139*, 3186–3195. [CrossRef]
6. Magallón, C.; Serrano-Plana, J.; Roldán-Gómez, S.; Ribas, X.; Costas, M.; Company, A. Preparation of a Coordinatively Saturated μ-H_2:H_2-Peroxodicopper(II) Compound. *Inorg.Chim. Acta* **2018**, *481*, 166–170. [CrossRef]
7. Paul, M.; Teubner, M.; Grimm-Lebsanft, B.; Buchenau, S.; Hoffmann, A.; Rübhausen, M.; Herres-Pawlis, S. Influence of the Amine Donor on Hybrid Guanidine-Stabilized Bis(μ-Oxido) Dicopper(III) Complexes and Their Tyrosinase-like Oxygenation Activity towards Polycyclic Aromatic Alcohols. *J. Inorg. Biochem.* **2021**, *224*, 111541. [CrossRef]
8. Tahsini, L.; Kotani, H.; Lee, Y.-M.; Cho, J.; Nam, W.; Karlin, K.D.; Fukuzumi, S. Electron-Transfer Reduction of Dinuclear Copper Peroxo and Bis-μ-Oxo Complexes Leading to the Catalytic Four-Electron Reduction of Dioxygen to Water. *Chem.-Eur. J.* **2012**, *18*, 1084–1093. [CrossRef]

9. Li, S.T.; Braun-Cula, B.; Hoof, S.; Limberg, C. Copper(I) Complexes Based on Ligand Systems with Two Different Binding Sites: Synthesis, Structures and Reaction with O_2. *Dalton Trans.* **2018**, *47*, 544–560. [CrossRef]
10. Kodera, M.; Kano, K. Reversible O_2-Binding and Activation with Dicopper and Diiron Complexes Stabilized by Various Hexapyridine Ligands. Stability, Modulation, and Flexibility of the Dinuclear Structure as Key Aspects for the Dimetal/O_2 Chemistry. *Bull. Chem. Soc. Jpn.* **2007**, *80*, 662–676. [CrossRef]
11. Dalle, K.E.; Gruene, T.; Dechert, S.; Demeshko, S.; Meyer, F. Weakly Coupled Biologically Relevant Cu^{II}_2 (μ-η^1:η^1-O_2) *Cis*-Peroxo Adduct That Binds Side-On to Additional Metal Ions. *J. Am. Chem. Soc.* **2014**, *136*, 7428–7434. [CrossRef] [PubMed]
12. Karlin, K.D.; Lee, D.-H.; Kaderli, S.; Zuberbühler, A.D. Copper Dioxygen Complexes Stable at Ambient Temperature: Optimization of Ligand Design and Solvent. *Chem. Commun.* **1997**, *5*, 475–476. [CrossRef]
13. Lohmiller, T.; Spyra, C.-J.; Dechert, S.; Demeshko, S.; Bill, E.; Schnegg, A.; Meyer, F. Antisymmetric Spin Exchange in a μ-1,2-Peroxodicopper(II) Complex with an Orthogonal Cu–O–O–Cu Arrangement and S = 1 Spin Ground State Characterized by THz-EPR. *JACS Au* **2022**, *2*, 1134–1143. [CrossRef] [PubMed]
14. Börzel, H.; Comba, P.; Hagen, K.S.; Kerscher, M.; Pritzkow, H.; Schatz, M.; Schindler, S.; Walter, O. Copper−Bispidine Coordination Chemistry: Syntheses, Structures, Solution Properties, and Oxygenation Reactivity. *Inorg. Chem.* **2002**, *41*, 5440–5452. [CrossRef] [PubMed]
15. Brückmann, T.; Becker, J.; Würtele, C.; Seuffert, M.T.; Heuler, D.; Müller-Buschbaum, K.; Weiß, M.; Schindler, S. Characterization of Copper Complexes with Derivatives of the Ligand (2-Aminoethyl)Bis(2-Pyridylmethyl)Amine (Uns-Penp) and Their Reactivity towards Oxygen. *J. Inorg. Biochem.* **2021**, *223*, 111544. [CrossRef]
16. Jacobson, R.R.; Tyeklar, Z.; Farooq, A.; Karlin, K.D.; Liu, S.; Zubieta, J. A Copper-Oxygen (Cu_2-O_2) Complex. Crystal Structure and Characterization of a Reversible Dioxygen Binding System. *J. Am. Chem. Soc.* **1988**, *110*, 3690–3692. [CrossRef]
17. Isaac, J.A.; Gennarini, F.; Lopez, I.; Thibon-Pourret, A.; David, R.; Gellon, G.; Gennaro, B.; Philouze, C.; Meyer, F.; Demeshko, S.; et al. Room-Temperature Characterization of a Mixed-Valent μ-Hydroxodicopper(II,III) Complex. *Inorg. Chem.* **2016**, *55*, 8263–8266. [CrossRef]
18. Isaac, J.A.; Thibon-Pourret, A.; Durand, A.; Philouze, C.; Le Poul, N.; Belle, C. High-Valence $Cu^{II}Cu^{III}$ Species in Action: Demonstration of Aliphatic C–H Bond Activation at Room Temperature. *Chem. Commun.* **2019**, *55*, 12711–12714. [CrossRef]
19. Isaac, J.A. Conception et Synthèse de Catalyseurs de Cuivre Bio-Inspirés Pour l'activation de Liaisons C-H. Ph.D. Thesis, Université Grenoble-Alpes, Grenoble, France, 2018.
20. Desimoni, G.; Faita, G.; Jørgensen, K.A. C2-Symmetric Chiral Bis(Oxazoline) Ligands in Asymmetric Catalysis. *Chem. Rev.* **2006**, *106*, 3561–3651. [CrossRef]
21. Walli, A.; Dechert, S.; Bauer, M.; Demeshko, S.; Meyer, F. BOX Ligands in Biomimetic Copper-Mediated Dioxygen Activation: A Hemocyanin Model: BOX Ligands in Copper-Mediated Dioxygen Activation. *Eur. J. Inorg. Chem.* **2014**, *2014*, 4660–4676. [CrossRef]
22. Dagorne, S.; Bellemin-Laponnaz, S.; Welter, R. Synthesis and Structure of Neutral and Cationic Aluminum Complexes Incorporating Bis(Oxazolinato) Ligands. *Organometallics* **2004**, *23*, 3053–3061. [CrossRef]
23. Bechlars, B.; D'Alessandro, D.M.; Jenkins, D.M.; Iavarone, A.T.; Glover, S.D.; Kubiak, C.P.; Long, J.R. High-Spin Ground States via Electron Delocalization in Mixed-Valence Imidazolate-Bridged Divanadium Complexes. *Nat. Chem.* **2010**, *2*, 362–368. [CrossRef] [PubMed]
24. Newkome, G.R.; Garbis, S.J.; Majestic, V.K.; Fronczek, F.R.; Chiari, G. Chemistry of Heterocyclic Compounds. 61. Synthesis and Conformational Studies of Macrocycles Possessing 1,8- or 1,5-Naphthyridino Subunits Connected by Carbon-Oxygen Bridges. *J. Org. Chem.* **1981**, *46*, 833–839. [CrossRef]
25. Boelrijk, A.E.M.; Neenan, T.X.; Reedijk, J. Ruthenium Complexes with Naphthyridine Ligands. Synthesis, Characterization and Catalytic Activity in Oxidation Reactions. *J. Chem. Soc. Dalton Trans.* **1997**, *23*, 4561–4570. [CrossRef]
26. Davenport, T.C.; Tilley, T.D. Dinucleating Naphthyridine-Based Ligand for Assembly of Bridged Dicopper(I) Centers: Three-Center Two-Electron Bonding Involving an Acetonitrile Donor. *Angew. Chem. Int. Ed.* **2011**, *50*, 12205–12208. [CrossRef] [PubMed]
27. Davenport, T.C.; Tilley, T.D. Dinuclear First-Row Transition Metal Complexes with a Naphthyridine-Based Dinucleating Ligand. *Dalton Trans.* **2015**, *44*, 12244–12255. [CrossRef]
28. Mirica, L.M.; Ottenwaelder, X.; Stack, T.D. Structure and Spectroscopy of Copper Dioxygen Complexes. *Chem. Rev.* **2004**, *104*, 1013–1045. [CrossRef]
29. Hatcher, L.Q.; Karlin, K.D. Oxidant Types in Copper–Dioxygen Chemistry: The Ligand Coordination Defines the Cu_n-O_2 Structure and Subsequent Reactivity. *J. Biol. Inorg. Chem.* **2004**, *9*, 669–683. [CrossRef]
30. Lucas, H.R.; Li, L.; Sarjeant, A.A.N.; Vance, M.A.; Solomon, E.I.; Karlin, K.D. Toluene and Ethylbenzene Aliphatic C−H Bond Oxidations Initiated by a Dicopper(II)-μ-1,2-Peroxo Complex. *J. Am. Chem. Soc.* **2009**, *131*, 3230–3245. [CrossRef]
31. Solomon, E.I.; Heppner, D.E.; Johnston, E.M.; Ginsbach, J.W.; Cirera, J.; Quyyum, M.; Kieber-Emmons, M.T.; Kjaergaard, C.H.; Hadt, R.G.; Tian, L. Copper Active Sites in Biology. *Chem. Rev.* **2014**, *114*, 3659–3853. [CrossRef]
32. Addison, A.W.; Rao, T.N.; Reedijk, J.; van Rijn, J.; Verschoor, G.C. Synthesis, Structure, and Spectroscopic Properties of Copper(II) Compounds Containing Nitrogen–Sulphur Donor Ligands; the Crystal and Molecular Structure of Aqua [1,7-Bis(N-Methylbenzimidazol-2′-Yl)-2,6-Dithiaheptane]Copper(II) Perchlorate. *J. Chem. Soc. Dalton Trans.* **1984**, *7*, 1349–1356. [CrossRef]

33. Halvagar, M.R.; Solntsev, P.V.; Lim, H.; Hedman, B.; Hodgson, K.O.; Solomon, E.I.; Cramer, C.J.; Tolman, W.B. Hydroxo-Bridged Dicopper(II,III) and -(III,III) Complexes: Models for Putative Intermediates in Oxidation Catalysis. *J. Am. Chem. Soc.* **2014**, *136*, 7269–7272. [CrossRef]
34. Kochem, A.; Gennarini, F.; Yemloul, M.; Orio, M.; Le Poul, N.; Rivière, E.; Giorgi, M.; Faure, B.; Le Mest, Y.; Réglier, M.; et al. Characterization of a Dinuclear Copper(II) Complex and Its Fleeting Mixed-Valent Copper(II)/Copper(III) Counterpart. *ChemPlusChem* **2017**, *82*, 615–624. [CrossRef]
35. Thibon-Pourret, A.; Gennarini, F.; David, R.; Isaac, J.A.; Lopez, I.; Gellon, G.; Molton, F.; Wojcik, L.; Philouze, C.; Flot, D.; et al. Effect of Monoelectronic Oxidation of an Unsymmetrical Phenoxido-Hydroxido Bridged Dicopper(II) Complex. *Inorg. Chem.* **2018**, *57*, 12364–12375. [CrossRef] [PubMed]
36. Mabbott, G.A. An Introduction to Cyclic Voltammetry. *J. Chem. Educ.* **1983**, *60*, 697. [CrossRef]
37. Elgrishi, N.; Rountree, K.J.; McCarthy, B.D.; Rountree, E.S.; Eisenhart, T.T.; Dempsey, J.L. A Practical Beginner's Guide to Cyclic Voltammetry. *J. Chem. Educ.* **2018**, *95*, 197–206. [CrossRef]
38. Robin, M.B.; Day, P. Mixed Valence Chemistry-A Survey and Classification. In *Adv Inorg Chem Radiochem*; Elsevier: Amsterdam, The Netherlands, 1968; Volume 10, pp. 247–422. ISBN 978-0-12-023610-7.
39. Stoll, S.; Schweiger, A. EasySpin, a Comprehensive Software Package for Spectral Simulation and Analysis in EPR. *J. Magn. Reson.* **2006**, *178*, 42–55. [CrossRef]
40. Brunschwig, B.S.; Creutz, C.; Sutin, N. Optical Transitions of Symmetrical Mixed-Valence Systems in the Class II–III Transition Regime. *Chem. Soc. Rev.* **2002**, *31*, 168–184. [CrossRef]
41. Winter, R.F. Half-Wave Potential Splittings $\Delta E_{1/2}$ as a Measure of Electronic Coupling in Mixed-Valent Systems: Triumphs and Defeats. *Organometallics* **2014**, *33*, 4517–4536. [CrossRef]
42. Warren, J.J.; Tronic, T.A.; Mayer, J.M. Thermochemistry of Proton-Coupled Electron Transfer Reagents and Its Implications. *Chem. Rev.* **2010**, *110*, 6961–7001. [CrossRef]
43. Sheldrick, G.M. A Short History of SHELX. *Acta Cryst. A* **2008**, *64*, 112–122. [CrossRef]
44. Dolomanov, O.V.; Bourhis, L.J.; Gildea, R.J.; Howard, J.A.K.; Puschmann, H. OLEX2: A Complete Structure Solution, Refinement and Analysis Program. *J. Appl. Crystallogr.* **2009**, *42*, 339–341. [CrossRef]